Effect of Segmented Electrode Length on the Performances of an Aton-Type Hall Thruster*

DUAN Ping (段萍), BIAN Xingyu (边兴宇), CAO Anning (曹安宁),
LIU Guangrui (刘广睿), CHEN Long (陈龙), YIN Yan (殷燕)

Department of Physics, Dalian Maritime University, Dalian 116026, China

Abstract The influences of the low-emissive graphite segmented electrode placed near the channel exit on the discharge characteristics of a Hall thruster are studied using the particle-in-cell method. A two-dimensional physical model is established according to the Hall thruster discharge channel configuration. The effects of electrode length on the potential, ion density, electron temperature, ionization rate and discharge current are investigated. It is found that, with the increasing of the segmented electrode length, the equipotential lines bend towards the channel exit, and approximately parallel to the wall at the channel surface, the radial velocity and radial flow of ions are increased, and the electron temperature is also enhanced. Due to the conductive characteristic of electrodes, the radial electric field and the axial electron conductivity near the wall are enhanced, and the probability of the electron-atom ionization is reduced, which leads to the degradation of the ionization rate in the discharge channel. However, the interaction between electrons and the wall enhances the near wall conductivity, therefore the discharge current grows along with the segmented electrode length, and the performance of the thruster is also affected.

Keywords: Hall thruster, segmented electrodes, particle-in-cell, ionization rate

PACS: *52.75.−d, 52.65.Rr*

DOI: 10.1088/1009-0630/18/5/14

(Some figures may appear in colour only in the online journal)

1 Introduction

The Hall thruster, a kind of small thrust device for spacecraft orbiting, has shown outstanding performances on the efficiency (above 60%), the specific impulse (in the order of 10^3 s) and the reliability, which has been widely applied to achieve the spacecraft propulsion tasks such as attitude control, station keeping, orbital transfer, etc [1−3]. The Hall thruster has a hollow and co-axial structure (shown in Fig. 1), and the propellants (usually Xenon atoms) enter the channel through the anode, collide with the electrons from the cathode, and then ionize into electrons and ions. As the electron Larmor radius is far smaller than the radial dimension of the thruster channel, the electrons take Hall drift movements under the axial electric field and radial magnetic field. Since the ion mass is far greater than the electron's, ions are accelerated and expelled out of the channel exit by the electric field to produce thrust [4]. The emitted ions are neutralized by the electrons released from the cathode to keep the thruster neutral. The regions where atoms are ionized and ions are accelerated are called the ionization region and acceleration region (shown in Fig. 2), respectively. The axial positions of the ionization and acceleration regions can directly affect the work efficiency and service life of a Hall thruster.

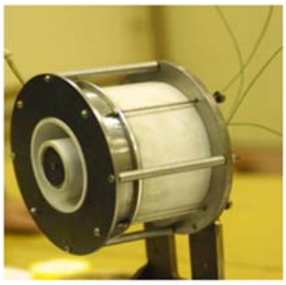

Fig.1 Schematic view of a Hall thruster

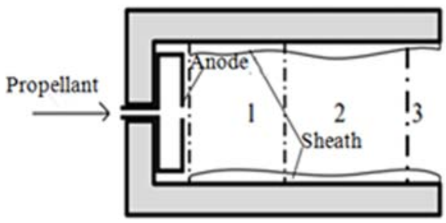

1 Near anode region, 2 Ionization region, 3 Acceleration region

Fig.2 The specific regions in the channel of a Hall thruster

In conventional Hall thrusters, which are also called stationary plasma thrusters (SPT), the electric field dis-

*supported by National Natural Science Foundation of China (Nos. 11375039 and 11275034) and the Key Project of Science and Technology of Liaoning Province, China (No. 2011224007) and the Fundamental Research Funds for the Central Universities, China (No. 3132014328)

tribution is controlled mainly by the magnetic field profile along a ceramic thruster channel [5]. However, due to the large divergence of the ion beam and the severe erosion of the channel walls, SPT cannot be widely used on satellites [6−8]. Therefore, scientists have proposed several kinds of methods to improve the performances of the Hall thruster, which also include the segmented electrode method. The main mechanism of a segmented electrode is to divide the dielectric wall into two parts, one part uses an insulating material and the other one is an electrode material. The segmented electrode Hall thruster was firstly proposed by the Princeton Plasma Physics Laboratory in 1998 [9,10]. Since then, the effects of segmented electrodes on the thruster have been studied both theoretically [11−13] and experimentally [14,15]. The results show that the application of segmented electrodes with a length of about several millimeters located near the channel exit can remarkably increase the electron temperature, and reduce the discharge current. Meanwhile, the electric potential distribution is also changed and plasma plume divergence is narrowed down at a low gas flow rate (<2 mg/s) [16−19]. Although a lot of works have been done by researchers on the effect of the segmented electrodes on certain kinds of Hall thruster, it is still needed to evaluate the segmented electrodes used in other kinds of Hall thrusters, such as the Aton type [20]. A number of investigations on Aton have been carried out by researchers from the Harbin Institute of Technology. The results, on the contrary, show that the plume divergence is actually increased when the segmented electrode is applied near the exit of the Hall thruster when the length of the electrode is longer than 2 mm. Besides, by comparing with non-segmented electrodes cases, the researchers found that the ion flow can be focused slightly only if the segmented electrode length $L_{\rm seg}$ <2 mm, and the performances of the Hall thruster will drop to some extent while using low-emissive graphite electrodes [21−23].

In this paper, a two-dimensional physical model aiming to describe the plasma motion in the discharge channel of the 1 kW/P70 Aton Hall thruster is established using the particle-in-cell (PIC) method. The potential, ion density, electron temperature, and ionization rate are investigated by comparing the different influences of segmented electrode (the segmented electrode length is set as $L_{\rm seg}$= 3 mm, 5 mm, 8 mm) and the non-segmented electrode ($L_{\rm seg}$= 0 mm) on the discharging process in the Hall thruster. The discharge voltage and the propellant flow of Xenon atoms are set to 350 V and 3 mg/s, respectively. Besides, the factors which lead to the increase of the discharge current are also analyzed.

2 Physical model and boundary conditions

2.1 Physical model

In this paper, two-dimensional spatial coordinates (axial z and radial r) and three-dimensional velocity coordinates (v_z, v_r, v_θ) are established according to the axisymmetric structure of the Hall thruster. The simulation region and the magnetic field configuration are shown in Fig. 3. The computation region is based on the actual discharge channel size of a P70 Aton Hall thruster, the channel length and width of which are z=30 mm and r=14 mm. The magnetic field strength is calculated by FEMM software.

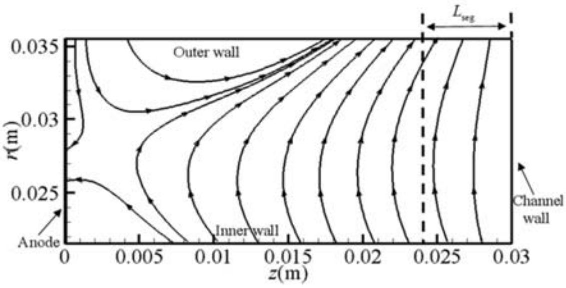

Fig.3 Simulation region and the magnetic field configuration

The Hall thruster discharge channel is numerically simulated via the Maxwell equations:

$$\nabla \times \mathbf{E} = -\frac{\partial \mathbf{B}}{\partial t}, \tag{1}$$

$$\nabla \cdot \mathbf{E} = \frac{\rho}{\varepsilon_0}, \tag{2}$$

where $\mathbf{E}$, $\mathbf{B}$, μ_0, ε_0 and ρ represent the electric field, the magnetic field, the vacuum permeability, the dielectric constant and the electric charge density, respectively. The Poisson equation can be obtained by the Maxwell equations:

$$\nabla^2 \Phi = -\frac{\rho}{\varepsilon_0}, \tag{3}$$

where Φ represents the potential.

In the cylindrical coordinate system, the 2D Poisson equation can be written as

$$\frac{1}{r}\frac{\partial}{\partial r}(r\frac{\partial \Phi}{\partial r}) + \frac{\partial^2 \Phi}{\partial z^2} = -\frac{e}{\varepsilon_0}(n_{\rm i} - n_{\rm e}), \tag{4}$$

where $n_{\rm i}$ and $n_{\rm e}$ are the ion and electron densities, and e is the unit charge.

The discharge channel is divided by identical mesh spaces along the axial direction z and the radial direction r. By applying the central difference method, Eq. (4) can be written as

$$\begin{aligned} &\frac{\Phi_{i+1,j} - 2\Phi_{i,j} + \Phi_{i-1,j}}{(\Delta z)^2} + \frac{1}{(\Delta r)^2} \\ &\quad \times \left(\frac{r_{i,j+\frac{1}{2}}}{r_{i,j}}\Phi_{i,j+1} - 2\Phi_{i,j} + \frac{r_{i,j-\frac{1}{2}}}{r_{i,j}}\Phi_{i,j-1}\right) \\ &\quad = -\frac{e\,(n_{\rm i} - n_{\rm e})_{i,j}}{\varepsilon_0}. \end{aligned} \tag{5}$$

Then Eq. (5) can be simplified as

$$\begin{aligned} &\frac{(\Delta r)^2}{(\Delta z)^2}(\Phi_{i+1,j} + \Phi_{i-1,j}) - 2\Big[1 + \frac{(\Delta r)^2}{(\Delta z)^2}\Big]\Phi_{i,j} \\ &+ \Big[\frac{r_{i,j+\frac{1}{2}}}{r_{i,j}}\Phi_{i,j+1} + \frac{r_{i,j-\frac{1}{2}}}{r_{i,j}}\Phi_{i,j-1}\Big] = -\frac{(n_{\rm i} - n_{\rm e})_{i,j}}{\varepsilon_0}\,(\Delta r)^2, \end{aligned} \tag{6}$$

where the Poisson equation becomes an elliptic equation, which is still difficult to solve directly. Therefore, by introducing the virtual time t', the Poisson Eq. (6) can be transformed into the following parabolic equation:

$$\frac{\partial \Phi}{\partial t'} = \nabla^2 \Phi - s, \tag{7}$$

where s is the source term corresponding to the right hand side of Eq. (5). When $t' \to \infty$, namely, $\partial\Phi/\partial t'=0$, Φ is the solution of the Poisson equation. Then, based on the Φ, the electric field which is used to calculate the movement of charged particles can be derived by the center differential method.

2.2 Equations of particle motions in the Hall thruster

For a single particle, the equations of movement for the particle with mass m and charge q in the electric and magnetic field ($\mathbf{E}$ and $\mathbf{B}$) are expressed as

$$\frac{\mathrm{d}}{\mathrm{d}t}(m\mathbf{v}) = q(\mathbf{E} + \mathbf{v} \times \mathbf{B}), \tag{8}$$

$$\frac{\mathrm{d}}{\mathrm{d}t}\mathbf{x} = \mathbf{v}, \tag{9}$$

where $\mathbf{v}$ is the velocity vector, and $\mathbf{x}$ is the position vector.

The Boris method is an explicit algorithm with a second order accuracy, which is generally used to solve the equations of particle motion. The velocity $\mathbf{v}^{t-\Delta t/2}$ is firstly changed to $\mathbf{v}^-$ through halftime electric field acceleration. Then according to the $\mathbf{v}^-$, $\mathbf{v}^+$ is obtained by calculating the rotating of particles in the magnetic field. At last, the new velocity $\mathbf{v}^{t+\Delta t/2}$ is derived after another half time of electric field acceleration. The specific formulas are

$$\mathbf{v}^- = \mathbf{v}^{t-\Delta t/2} + \frac{e\Delta t \mathbf{E}^t}{2m}, \tag{10}$$

$$\mathbf{v}' = \mathbf{v}^- + \mathbf{v}^- \times t^t, \tag{11}$$

$$\mathbf{v}^+ = \mathbf{v}^- + \mathbf{v}' \times \frac{2t^t}{1 + t^t \cdot t^t}, \tag{12}$$

$$\mathbf{v}^{t+\Delta t/2} = \mathbf{v}^+ + \frac{e\Delta t \mathbf{E}^t}{2m}, \tag{13}$$

where $t^t = e\Delta t \mathbf{B}^t / (2m)$, and superscript t represents the corresponding time step.

2.3 Boundary conditions

The boron nitride (BN) ceramic is adopted as the insulating wall material for the Hall thruster. According to the secondary electron emission model proposed by Morozov [24], when an electron interacts with the wall, one of the following four events may occur for the electron: the electron either is absorbed by the wall, reflected elastically, knocks out one electron, or knocks out two electrons. The corresponding probabilities of those events are

$$W_0(\varepsilon) = P_0 \exp\left(-\frac{\varepsilon^2}{\alpha_0}\right), \tag{14}$$

$$W_r(\varepsilon) = P_r \exp\left(-\frac{\varepsilon^2}{\alpha_r^2}\right), \tag{15}$$

$$W_2(\varepsilon) = 1 - \exp\left(-\frac{\varepsilon^2}{\alpha_2^2}\right), \tag{16}$$

$$W_1(\varepsilon) = 1 - W_0(\varepsilon) - W_r(\varepsilon) - W_2(\varepsilon). \tag{17}$$

The parameters for the BN material are P_0=0.5, α_0=43.5, P_r=0.5, α_r=30, α_2=127.9.

Graphite, as a conductor, also exists as a secondary electron emission phenomenon, and the secondary electron emission model is the same as that of BN. Parameters for the graphite electrode are as follows: P_0=0.58, α_0=2422, P_r=0.42, α_r=30, and α_2=208.

For its conductive characteristic, the graphite electrode is treated by a conductor boundary condition which was proposed by Szabo [25] modeling the potential on the floating conductive wall surface:

$$\Phi_m = \frac{Q_\mathrm{e}}{C}, \tag{18}$$

where Q_e is the net charge deposited on the wall and the capacitance $C = 10^{-10}$ F.

3 Simulation results and analysis

3.1 Effects of segmented electrode length on the distribution of accelerating field and ion focusing

As graphite electrode material has different conductive characteristic compared to boron nitride material, the segmented electrode will have an effect on the distribution of ion density n_i and potential Φ. Fig. 4(a) represents the distributions of electron density and potential when the segmented electrode is applied. Region I marked in Fig. 4(a) represents the ionization zone and region II is the acceleration zone. It can be seen that with the increasing of segmented electrode length, the equipotential lines become more bent and form a convex shape towards the channel exit. Meanwhile, due to the freely moving electrons on the electrode surface caused by the conductive characteristic of graphite, the electric potential on the electrode surface is equal everywhere, therefore the equipotential lines nearby become parallel to the wall surface approximately according to the continuity of plasma parameters among wall surface, near-wall sheath [26,27] and channel plasma. As the distribution of electric potential is increasingly convex towards the exit, the radial electric potential drop in the acceleration region grows and the radial ion energy increases due to the radial electric potential, therefore the radial ion velocity is enhanced. Fig. 4(b) shows the distribution of radial ion velocity v_r for the case of the segmented electrode. It indicates that the area of the high ion velocity region as well as the radial ions

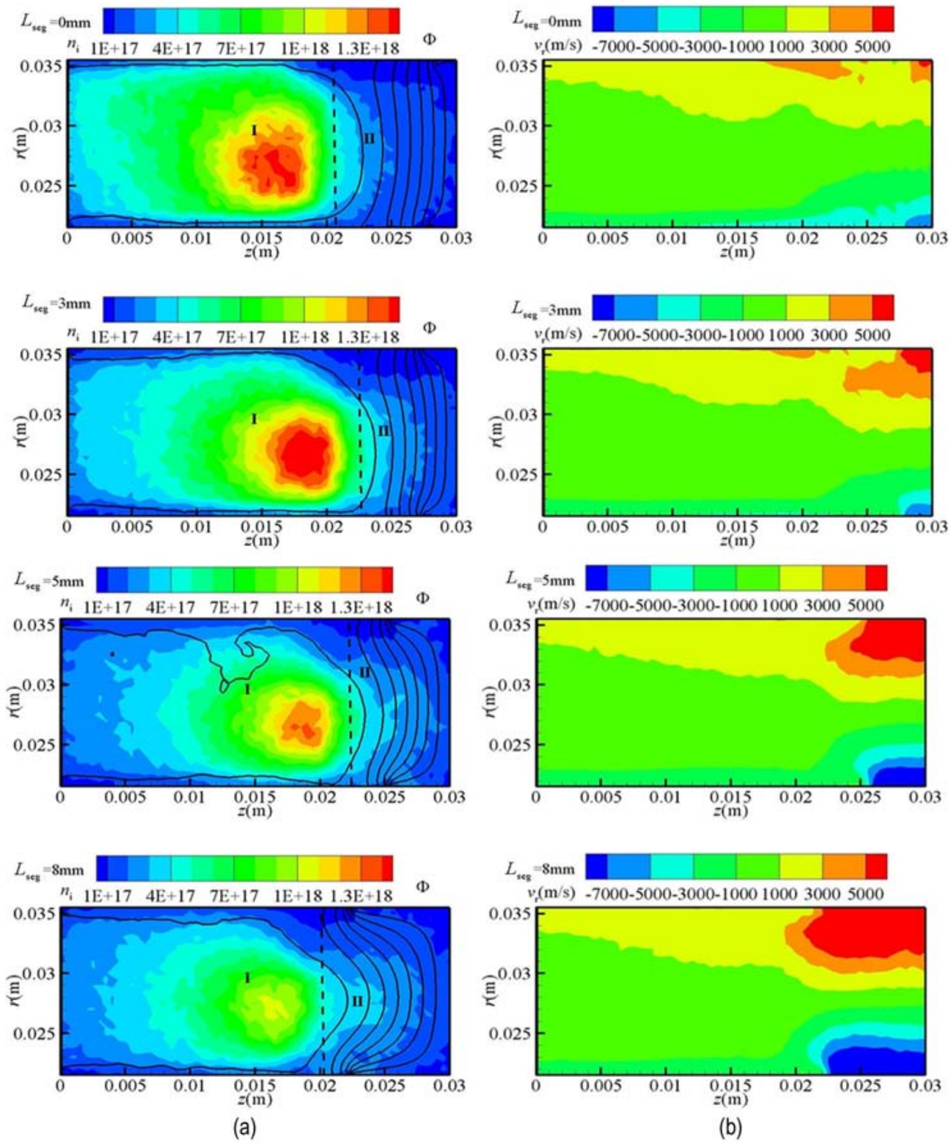

Fig.4 The spatial distribution of plasma parameters such as (a) equipotential lines, ion density and (b) radial ion velocity for low-emissive electrode cases, $L_{\rm seg}$= 0 mm, 3 mm, 5 mm, 8 mm

flow grows along with the increasing of segmented electrode length. Because the increasing of ion radial velocity has a negative effect on the ion focusing, the ions scattering angle in the exit plane will be greater and thrust will be weakened. The interaction between ions and wall will lead to the corrosion of surface material, so the efficiency and performance of a Hall thruster will drop predictably.

3.2 Effects of segmented electrode length on the axial electron temperature

As graphite has a lower secondary electron emission coefficient compared to BN material [23], it will have a lower probability to knock out the secondary electrons when the incident electrons with the same energy interact with graphite than BN materials. The secondary electrons have a lower electron temperature than incident electrons, therefore they have significant influences on the electron temperature of the main plasma region in the channel. Fig. 5 shows the distribution of electron temperature $T_{\rm e}$ along the axial for the cases of segmented electrodes. It can be seen that with the increasing of segmented electrode length, the axial position of the peak electron temperature moves towards the anode as long as $L_{\rm seg} \leq 3$ mm, but it moves back towards the channel exit when the segmented electrode length continues to grow. The moving direction is the same as that of the ionization region shown in Fig. 4(a). Since the equipotential lines which are convex towards the exit plane increase the radial electric potential drop of the acceleration region, part of the low energy electrons in the plasma mainstream area will be prevented from moving towards the wall. Meanwhile, the lower secondary electron emission coefficient of graphite reduces the loss of the electron energy during their interaction with the wall. Therefore, the total loss of the electron energy reduces, and the electron temperature of the channel keeps growing with the increasing of the segmented electrode length.

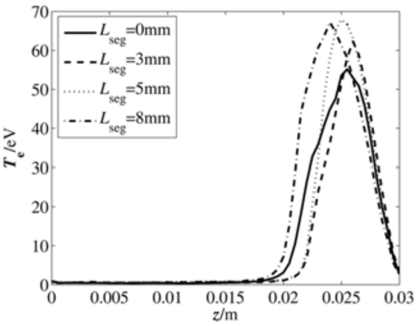

Fig.5 The distribution of the electron temperature T_e along the axial z for the cases of $L_{seg} = 0$ mm, 3 mm, 5 mm, 8 mm

3.3 Effects of segmented electrode length on the propellant ionization rate

For the Xenon propellant,the ionization rate can be expressed as [28]

$$S_i(z) = \begin{cases} 0, & T_e < T^* \\ n_a(z)n_e(z)\beta_0(z)(\frac{T_e}{T^*} - 1), & T_e > T^* \end{cases}, \quad (19)$$

where n_e is the electron density, $n_a(z)$ is the atom density, while β_0 and T^* are constants. Here we use $\beta_0 = 2.2 \times 10^{-14}$ m^{3}s^{-1}, and $T^* = 4$ eV. According to Eq. (19), the ionization rate can be approximately decided using Eq. (20) when the atom density change can be neglected.

$$S_i(z) = n_e(z)\beta_0(z)(T_e/T^* - 1). \quad (20)$$

Eq. (20) indicates that the ionization rate would increase if the electron temperature grows.

Fig. 6 shows the axial distributions of propellant ionization rate S_i for the different lengths of segmented electrode, it indicates that the axial position of the peak ionization rate has the same moving direction as that of the ionization region shown in Fig. 4(a). However, different from the results of Eq. (20), the ionization rate decreases with the increasing of electron temperature when the segmented electrode method is applied, which is caused by the radial variation of axial electric field.

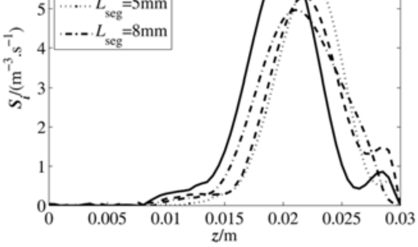

Fig.6 Axial distribution of propellant ionization rate S_i for the cases of segmented electrode lengths $L_{seg} = 0$ mm, 3 mm, 5 mm, 8 mm

Fig. 7 shows the distribution of axial electric field E_z for the different cases of segmented electrode, it can be seen that with the increasing of the segmented electrode length, the radial variation of the axial electric field inside the discharge channel increases gradually. The stability of electron Hall drift can be easily broken by the variation of the axial electric field, which leads to the increase of near wall conductivity caused by axial conduction of electrons near the wall surface. The collision probability between ions and atoms declines with the increasing of near wall conductivity, which finally leads to the reduction of the ionization rate.

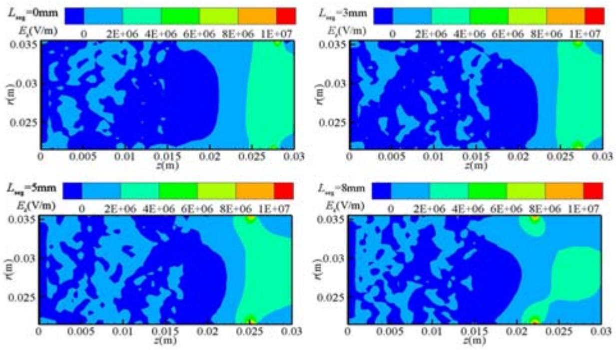

Fig.7 The variation of axial electric field for the cases of segmented electrode lengths $L_{seg} = 0$ mm, 3 mm, 5 mm, 8 mm

3.4 Effects of segmented electrode length on the discharge current

The discharge current is an important parameter to reflect the macro-performance of a Hall thruster. Discharge current can be obtained by the statistical number of electrons on the anode plane. Fig. 8 shows the discharge current versus the segmented electrode length, which indicates that the discharge current (namely I_d) increases with the increasing of the segmented electrode length, this result agrees with the experiment results qualitatively [29]. Generally, there are two reasons causing the increase of the discharge current, one of which is the increasing of the near wall conductivity current and the other is the directional movements of electrons on the electrode surface.

The formula of near wall conductivity current can be expressed as [30]

$$I_w = \frac{\bar{\sigma} j_{ew}}{\omega_c^2} \frac{e^2}{m_e} E_z = \bar{\sigma} j_{ew} m_e n_e \frac{E_z}{B^2}, \quad (21)$$

where j_{ew} is the electron flux flowing to the wall surface, ω_c is the cyclotron frequency of the electron, and $\bar{\sigma}$ is the total emission coefficient of the secondary electron. The secondary electron emission flux increases with the growth of the electron flux flowing to the wall surface, so the near wall conductivity current is proportional to the secondary electron emission flux according to Eq. (21). When the method of the graphite segmented electrode is applied, the total secondary electron flux grows [21] as well as the near wall conductivity current. Besides, due to the conductive characteristic of graphite, the electrons on the electrode surface generate directional movements towards the anode under the axial electric field, which contribute to the discharge current.

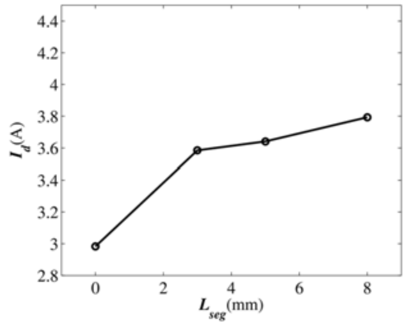

Fig.8 Discharge current I_d versus segmented electrode length L_seg

4 Conclusions

The low-emissive electrode placed near the exit of the P70 Hall thruster can promote the equipotential lines bending toward the channel exit. Due to the conductive characteristic of graphite electrodes, the electrode surface equipotential lines are parallel to the wall approximately, which leads to the increase of the radial electric potential drop and the area of high ion velocity region, and the radial ion flow also grows along with the increasing of segmented electrode length. Meanwhile, the low emission of the graphite electrode significantly increases the electron temperature. However, due to the convex topology of the electric potential at the channel exit, the radial variation of the axial electric field increases. Therefore, the stability of the electric drift motion will be broken, and the axial conductivity of electrons will be increased, which reduces the ionization rate. Due to the growing of the total secondary electron flux, the near wall conductivity increases, and the directional movements of electrons are enhanced by the increasing axial electric field, therefore the discharge current increases with the increasing of segmented electrode length. In conclusion, the performance of the Hall thruster drops with the increasing of the segmented electrode length.

References

1 Morozov A I. 2003, Plasma Phys. Rep., 29: 235

2 Mao G W, Han X W, Yang J, et al. 2000, Journal of Propulsion Technology, 21: 1 (in Chinese)

3 Yu L H, Huang Q D, Zhang Y. 2014, Research on the Application of Electric Propulsion Technology in Small Satellite. Proceeding of the 10th Chinese Electric Propulsion Conference, Shanghai, China, paper No.43 (in Chinese)

4 Mao G W, Tang J L. 2009, Spacecraft propulsion system and its application. Northwestern Polytechnical University Press, Xi'an, China (in Chinese)

5 Raitses Y, Smirnov A, Staack D, et al. 2006, Segmented Electrode in Annual and Cylindrical Hall Thrusters. Proceedings of the 42nd Joint Propulsion Conference and Exhibit, July 9-12, Sacramento, the United States. AIAA 2006-4471

6 Katz I, Jongeward G, Davis V, et al. 2001, A Hall effect thruster plume model including large-angle elastic scattering. Proceedings of the 37th Joint Propulsion Conference and Exhibit, July 8-11, Salt-Lake City, the United States. AIAA 2001-3355

7 Raitses Y, Staack D, Keidar M, et al. 2005, Phys. Plasmas, 12: 057104

8 Garrigues L, Hagelaar G J M, Bereilles J, et al. 2003, Phys. Plasmas, 10: 4886

9 Bechu S, Pdrot C and Gascon. 1999, Operating Model Investigation of Laboratory Stationary Plasma Thruster. Proceedings of the 35th Joint Propulsion Conference and Exhibit, June 20-24, Los Angeles, the United States. AIAA 1999-2567

10 Raitses Y, Dorf L A, Litvak A A, et al. 2000, J. Appl. Phys., 88: 1263

11 Fruchtman A, Fisch N J and Raitses Y. 2001, Phys. Plasmas, 8: 1048

12 Raitses Y, Keidar M, Staack D, et al. 2002, J. Appl. Phys., 92: 4906

13 Keidar M, Gallimore A, Raitses Y, et al. 2004, Appl. Phys. Lett., 85: 2481

14 Raitses Y, Staack D and Fisch N. 2002, Proceedings of the 38th Joint Propulsion Conference and Exhibit, July 7-10, Indianapolis, the United States

15 Diamant K, Pollard J, Cohen R, et al. 2004, Proceedings of the 40th Joint Propulsion Conference, July 11-14, Fort Lauderdale, the United States

16 Raitses Y, Dorf L A, Litvak A A, et al. 2000, J. Appl. Phys., 88: 3

17 Raitses Y, Zeidar A A, Staack D, et al. 2002, J. Appl. Phys., 92: 9

18 Raitses Y, Staack D, Dunaevsky A, et al. 2006, J. Appl. Phys., 99: 036103

19 Raitses Y, Smirnov A, Staack D, et al. 2006, Phys. Plasmas, 13: 014502

20 Yu D R, Li J, Liu H, et al. 2009, Contrib. Plasma Phys., 49: 6

21 Yu D R, Qing S W, Liu H, et al. 2011, Contrib. Plasma Phys., 51: 955

22 Qing S W, E P, Duan P, et al. 2013, Chinese Physics B, 22: 085203

23 Qing S W, E P, Xia G Q, et al. 2014, J. Appl. Phys., 115: 033301

24 Yu D R, Zhang F K, Liu H, et al. 2008, Phys. Plasmas, 15: 104501

25 Szabo J J. 2001, Fully Kinetic Numerical Modeling of a Plasma Thruster [Ph.D]. Massachusetts Institute of Technology, Massachusetts, the United States

26 Duan P, Qin H J, Zhou X W, et al. 2014, Chinese Physics B, 23: 075203

27 Duan P, Qin H J, Zhou X W, et al. 2014, Acta Phys. Sin., 63: 085204 (in Chinese)

28 Morozov A I and Savelev V V. 2000, Plasma Phys. Rep., 26: 875

29 Staack D, Raitses Y and Fisch N J. 2003, Proceedings of the 28th International Electric Propulsion Conference, March 17-21, Cleveland, the United States

30 Degond P A. 1998, Journal of Applied Mathematics, 58: 1138

(Manuscript received 6 September 2015)
(Manuscript accepted 27 October 2015)
E-mail address of corresponding author CHEN Long:
chenlong@dlmu.edu.cn